ACS APPLIED MATERIALS & INTERFACES

Research Article

www.acsami.org

Role of Specific Interfacial Area in Controlling Properties of Immiscible Blends of Biodegradable Polylactide and Poly[(butylene succinate)-co-adipate]

Vincent Ojijo,[†,‡] Suprakas Sinha Ray,[*,†,§,⊥] and Rotimi Sadiku[‡]

[†]DST/CSIR National Centre for Nano-Structured Materials, Council for Scientific and Industrial Research, 1-Meiring Naude Road, Brummeria, Pretoria 0001, South Africa

[‡]Division of Polymer Technology, Department of Mechanical Engineering, Tshwane University of Technology, Pretoria 0001, South Africa

[§]Department of Applied Chemistry, University of Johannesburg, Doornfontein 2028, Johannesburg, South Africa

[⊥]Department of Chemistry, King Abdulaziz University, Jeddah 21589, Kingdom of Saudi Arab

ABSTRACT: Binary blends of two biodegradable polymers: polylactide (PLA), which has high modulus and strength but is brittle, and poly[(butylene succinate)-co-adipate] (PBSA), which is flexible and tough, were prepared through batch melt mixing. The PLA/PBSA compositions were 100/0, 90/10, 70/30, 60/40, 50/50, 40/60, 30/70, 10/90, and 0/100. Fourier-transform infrared measurements revealed the absence of any chemical interaction between the two polymers, resulting in a phase-separated morphology as shown by scanning electron microscopy (SEM). SEM micrographs showed that PLA-rich blends had smaller droplet sizes when compared to the PBSA-rich blends, which got smaller with the reduction in PBSA content due to the differences in their melt viscosities. The interfacial area of PBSA droplets per unit volume of the blend reached a maximum in the 70PLA/30PBSA blend. Thermal stability and mechanical properties were not only affected by the composition of the blend, but also by the interfacial area between the two polymers. Through differential scanning calorimetry, it was shown that molten PBSA enhanced crystallization of PLA while the stiff PLA hindered cold crystallization of PBSA. Optimal synergies of properties between the two polymers were found in the 70PLA/30PBSA blend because of the maximum specific interfacial area of the PBSA droplets.

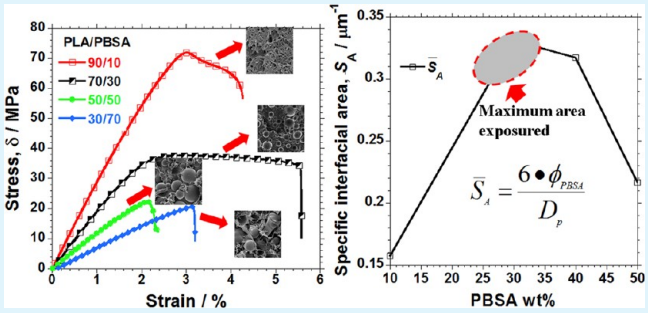

KEYWORDS: *interfacial area, phase morphology, polylactide/poly[(butylene succinate)-co-adipate] blends, thermal and mechanical properties*

1. INTRODUCTION

Because of growing environmental concerns and limited petroleum resources, biodegradable polymers, more so from renewable resources, have continued to receive considerable attention. In this regard, one biodegradable and biocompatible polymer widely regarded as a green polymer suitable as an alternative to the nonbiodegradable polymers is polylactide (PLA).[1] PLA is a linear aliphatic thermoplastic polyester, generally produced through ring-opening polymerization of the lactide monomer, obtained from fermentation of renewable resources such as corn.[2,3] PLA has found a number of uses, mainly in biomedical applications[4−7] and as an advanced environmentally benign material.[2,8−10] When compared to other polymers, such as high density polyethylene (HDPE), polystyrene (PS), polypropylene (PP), and polyethylene terephthalate (PET), PLA has good mechanical, optical, physical, and barrier properties. Tensile strength of PLA of approximately 44−82 MPa has been reported to be close to that of PS.[2,11,12] With the envisaged further reduction in prices of the industrial grade PLA and its high mechanical strength, PLA is expected to be a sustainable alternative to the traditional petroleum-based plastics. However, despite the good properties, its low flexibility (elongation at break for PLA is approximately 2.5−6%)[13] and low impact strength could limit its applications. Thus, researchers have looked for different ways to toughen PLA without necessarily losing its inherent properties.

Blending PLA with flexible polymers is a practical and economical way to obtain toughened PLA products. The brittleness could be overcome through blending PLA with more ductile and still biodegradable polymers, such as polycaprolactone (PCL),[14−23] poly(butylene adipate-*co*-tephthalate),[24−28] polyhydroxy-alkanoates,[29−31] and poly(butylene succinate).[31−37] In the current study, ductile poly[(butylene succinate)-co-adipate] (PBSA) was used to modify the properties of PLA. PBSA is an environmentally benign biodegradable thermoplastic polyester

Received: September 4, 2012
Accepted: November 13, 2012
Published: November 13, 2012

   dx.doi.org/10.1021/am301842e | *ACS Appl. Mater. Interfaces* 2012, 4, 6690−6701

made of butylene succinate adipate random copolymer. It is chemically synthesized by polycondensation of 1,4-butanediol with succinic and adipic acids[38−40] and has an elongation-at-break of over 300%, although its strength is quite low, approximately 20 MPa, just as its modulus is less than 400 MPa. Because of the complementary nature of the properties of PLA and PBSA, blending the two provides a simple way to modify the properties of both for various purposes.

A challenge that exists for the immiscible blends like PLA and PBSA is the phase-separated morphology, which leads to deterioration of desirable properties. The mixing process in melt-blended samples plays a key role in the determination of the morphology, as is the viscosity ratio between the two polymers and volume fraction for each. Moreover, the crystallization phenomena of the two polymers are disparate, with PBSA crystallizing very fast while PLA crystallizes very slowly and at different (higher) temperatures. Annealing of the blends to allow crystallization of the PLA component would, therefore, lead to probable further phase separation and deterioration of certain properties, e.g. strength. However, even though they are immiscible, some level of intermingling of chains of both polymers at the interface is expected. Maximising the benefits from the two polymers would, therefore, require that the dispersed phase is not only small in size, but also the droplet surface area per unit volume of the blend volume is the highest it can be.

Even though a few studies have appeared on the PLA/PBSA blend system,[41−48] none of them dealt specifically with the correlation between the morphology (hence specific interfacial area) and other properties of the blends. Similarly, to the best of our knowledge, none of those studies have shown the effect of crystallization of PLA components through annealing on the morphology and properties of the blends, which for a slow crystallizing polymer like PLA, can play a significant role. The only work on neat PLA/PBSA blend prepared through melt extrusion was reported by Lee and Lee.[41] They reported the thermal, rheological, morphological, and mechanical properties of binary PLA/PBSA blend, but did not attempt to explain the morphology-property relationship.

In the current study, an attempt is made at correlating the phase morphology with the properties of the PLA/PBSA blend. A polarized optical microscope (POM) equipped with a heating stage for studying melt-state morphology, and SEM for solid-state ultrastructure were used to examine the effects of composition on the blend-phase morphology. Additionally, due to the immiscibility of the two polymers, the concept of specific interfacial area (interfacial area of dispersed droplets per unit volume of the blend) is introduced and used as a yardstick to gauge the composition with the best synergies. Moreover, crystallization process through annealing and its effects on the mechanical properties are discussed.

Therefore, the objectives of the current study are to relate qualitatively phase morphology with the thermal and mechanical properties of the PLA/PBSA blends, and to explain the role of the specific interfacial area in controlling those properties. From the observations made, the appropriate blend composition suitable for further compatibilization is advanced.

2. EXPERIMENTAL SECTION

2.1. Materials. The PLA used in the study is a commercial grade (PLA 2002D), obtained from Natureworks, LLC. (USA). It had a D-isomer content of about 4%. On the other hand, PBSA, with the designation BIONOLLE #3001, was obtained from Showa High Polymer (Japan). The glass transition temperatures (T_g), the melting temperatures (T_m), molecular weights (M_w), and the densities (ρ) of the two polymers as obtained from the manufacturers are summarized in Table 1. The zero shear viscosities (η_o) of the two polymers at 185 °C are also shown in the table.

Table 1. Properties of PLA and PBSA

material	M_w (kg mol^{-1})	T_g (°C)	T_m (°C)	η_o (Pa S)	ρ (g cm^{-3})
PLA	235	60	153	1180	1.24
PBSA	190	−43.8	83.1 and 94.5*	80.8	1.23

*The PBSA had two melting points. PBSA inherently has more than one melting peak because of the fact that a portion of crystals formed are not stable and undergo the melt−recrystallization−melt phenomenon upon heating. The unstable crystal first melts, then recrystallizes, and eventually melts at a higher temperature.

2.2. Preparation of the Blends. Before processing, PLA was dried at 80 °C under vacuum for 36 h, whereas PBSA was dried at 60 °C under vacuum for 12 h. PLA/PBSA blends with various weight ratios (100/0, 90/10, 70/30, 60/40, 50/50, 40/60, 30/70, 10/90, and 0/100) were melt compounded in a batch mixer, HAAKE PolyLab OS Rheomix (Thermo Electron Co., USA) operated at a rotor speed of 60 rpm and a temperature of 185 °C (set temperature) for 8 min. The blends were then compression molded into various specimen forms using a Carver laboratory press at 185 °C, and later cooled to room temperature.

2.3. Characterization. To check for any chemical interaction between PLA and PBSA, attenuated total reflectance (ATR) Fourier-transform infrared (FT-IR) spectroscopy using a Perkin-Elmer Spectrum 100 spectrometer in the wavelength region of between 550 and 4000 cm^{-1} was performed on the blends.

Dog-bone shaped samples were annealed at 80 °C for 15 h and subsequently subjected to tensile fracture. The tensile-fractured surfaces of the PLA/PBSA blends were sputter-coated with gold/palladium alloy to minimise charging, and their surface morphology of the PLA/PBSA blends was studied using a scanning electron microscope (SEM, AURIGA CrossBeam®Workstation from Carl Zeiss, Germany) at an accelerating voltage of 3 kV. On the other hand, morphology of the molten samples was studied by polarized optical microscope (POM) equipped with a heating stage. Samples sandwiched between two glass coverslips were heated on Linkam THMS heating stage (Linkam Scientific Instruments, Ltd.) from room temperature to 190 °C at a rate of 10 °C/min, and held at this temperature for 5 min before cooling at the same rate to 120 °C to allow only the PLA component to crystallize. They were then held isothermally for 60 min, during which time, images were taken using a Carl Zeiss imager Z1M POM.

Differential scanning calorimetry (DSC) measurements of samples weighing approximately 11.7 mg were taken on a DSC-Q2000 instrument (TA Instruments, USA) in the temperature range of -65 to 190 °C under a nitrogen atmosphere. The samples were tested at the same heating and cooling rate of 10 °C/min in three consecutive scans: heating, cooling, and heating. While the first heating scan erased the previous thermal history of the samples, the second heating scan was used to determine the glass transition temperature (T_g), crystallization temperature (T_c), cold crystallization temperature (T_{cc}), enthalpy of crystallization (ΔH_c), enthalpy of cold crystallization (ΔH_{cc}), melting points (T_m), and heat of fusion (ΔH_m). To study the cold crystallization of PBSA in the presence of amorphous PLA, DSC with a ballistic cooling system was used (PerkinElmer HyperDSC 8500). The pre-weighed samples were heated to 190 °C, held for 5 min before being ballistically cooled to −150 °C so as to keep PLA and PBSA in their amorphous states. Then, heating was done at 10 °C/min to 190 °C to study the cold crystallization of PBSA in the presence of amorphous PLA.

Thermogravimetric analyses (TGA) were conducted on a TG analyser (model Q500, TA Instruments). Samples weighing approximately 5−9 mg were heated from room temperature to 900 °C at a heating rate of 10 °C/min under air. To obtain characteristic thermal stability indicators, such as the onset degradation temperature, and to

make the data statistically relevant, three individual tests were carried out per sample and the average value reported.

Dynamic mechanical analysis (DMA) was carried out using a PerkinElmer DMA 8000 analyser in the dual cantilever bending mode. The temperature dependence of the storage modulus (E') was measured at a frequency of 1 Hz. The strain amplitude was set at 0.05%, and the heating rate was 2 °C/min in the temperature range of −90 to +105 °C.

Tensile tests to determine the modulus, yield strength, and elongation-at-break were carried out using an Instron 5966 tester (Instron Engineering Corporation, USA) with a load cell of 10 kN, according to ASTM 638D standards. This was carried out under tension mode at a single strain rate of 5 mm/min at room temperature. Two dog-bone shaped samples were analyzed: (i) nonannealed and (ii) annealed at 80 °C for 15 h under vacuum. The results presented are an average of at least six individual tests per sample.

3. RESULTS AND DISCUSSION

3.1. Phase Morphology. The FTIR spectra of neat PLA, PBSA, and 70PLA/30PBSA blends are shown in Figure 1. PLA

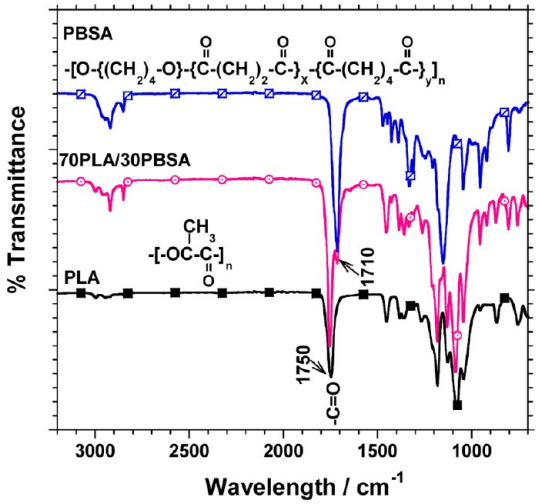

Figure 1. Fourier-transform infrared spectra of neat PLA, PBSA, and 70PLA/30PBSA blend. The chemical formulae of both polymers are also shown.

and PBSA are characterized by intense absorption bands at 1750 and 1710 cm^{-1}, respectively, due to the stretching of the carbonyl group (C═O) available in both polyesters. The spectrum of the neat blend comprising 70 wt % PLA was basically an overlap of the individual spectra of PLA and PBSA (as shown by the presence of both 1750 and 1710 cm^{-1} absorption peaks) of PLA and PBSA, indicating insignificant chemical interaction between the two polymers. As a result, the two polymers tended to form immiscible blends characterized by two-phase morphologies as shown in Figure 2.

Generally, the size of the droplets of the dispersed phase (PBSA) increased as the PBSA content was increased (refer to parts a−d in Figure 2) and so was the spread of the droplet sizes around a mean value. At a PLA/PBSA ratio of 40/60, a co-continuous morphology was obtained, as shown in Figure 2e. A low-magnification SEM image of the same sample at a different location clearly shows the co-continuity in the structure (refer to Figure 2e′). For the 30/70 (refer to Figure 2f) and 10/90 (refer to Figure 2g) samples, PLA formed a discrete dispersed phase, although the droplet sizes were larger than those of the respectively opposite compositions, *viz.* 70/30 (refer to Figure 2b) and 90/10 (refer to Figure 2a).

Two processes played critical roles in the formation of the morphologies observed in Figure 2: (i) mixing and (ii) annealing. For flow-induced structural evolution in immiscible polymer blends, factors, such as the mixing conditions, interfacial tension between the phases, volume fraction, and viscosity ratio of the constituent polymers, control the resultant morphology. In the current study, all samples were prepared similarly in a batch mixer with a rotor speed of 60 rpm, at a temperature of 185 °C for 8 min. The different morphologies observed in Figure 2 are, therefore, the result of the different volume fractions and subsequent phase separation during annealing. The structures induced through the mixing process tend to be unstable for immiscible blends and this phenomenon may be made worse through crystallization during the annealing process.

Briscoe et al.[49] summarize the factors that influence the shear strain required to produce break-up in a steady-state laminar flow as: (i) the dispersed and continuous phase viscosities, η_d and η_m, respectively, (ii) the initial radius of the droplet, R, and (iii) the interfacial tension between the matrix and droplet, σ. For Newtonian flow, droplet deformation is governed by two dimensionless numbers: the viscosity ratio $p = (\eta_d/\eta_m)$ and the capillary number, C_a, given by the ratio of deforming viscous stress to the restoring stress from the interfacial tension in the following equation[49]

$$C_a = \frac{\eta_m \dot{\gamma}}{\sigma/R} \quad (1)$$

where η_m is the viscosity of major matrix, $\dot{\gamma}$ is the shear strain rate, R is the radius of dispersed phase, and σ is the interfacial tension. The numerator is the deforming stress, whereas the denominator is the restoring interfacial stress.

At the processing temperature of 185 °C, the viscosity of PBSA was much lower than that of PLA (refer to Table 1). Therefore, better mixing should then be realized in the PLA-dominated compositions than in the opposite, but corresponding, PBSA-dominated compositions. In cases where PBSA formed the major matrix, it failed to deform PLA, and this explains why PLA droplet size, for instance the 30/70 sample (refer to Figure 2f), was larger than PBSA droplets in 70/30 sample (refer to Figure 2g).

To check the miscibility of the two polymers in the melt state, POM images were taken for selected samples at 190 °C and after crystallization of the PLA component in the presence of molten PBSA. Indeed, the immiscibility of the two polymers is also evident even in a molten state, as illustrated by the micrograph in Figure 3a. At 30 wt % of PBSA, the blend shows distinct island-sea morphology in the molten state, similar to the one observed with SEM (refer to Figure 2b). Crystallizing the PLA component at 120 °C when the PBSA is still in a molten state, similarly results in a phase-separated morphology, as shown by the micrograph in Figure 3a′. However, at a higher concentration of PBSA (50 wt %), a co-continuous structure was formed in the melt, as shown in Figure 3b. Crystallizing PLA component at 120 °C confirms the co-continuity in the structures, as shown in Figure 3b′. This structure is, however, unstable during the mixing process, and this explains why a different morphology for the corresponding sample was observed in the tensile-fractured specimens (refer to SEM image in Figure 2 (d)). Most importantly, for the 70PLA/30PBSA sample, even in the melt, coalescence of the PBSA phase was not observed, as opposed to the co-continuous morphology seen when PBSA content was increased (50PLA/50PBSA

dx.doi.org/10.1021/am301842e | ACS Appl. Mater. Interfaces 2012, 4, 6690−6701

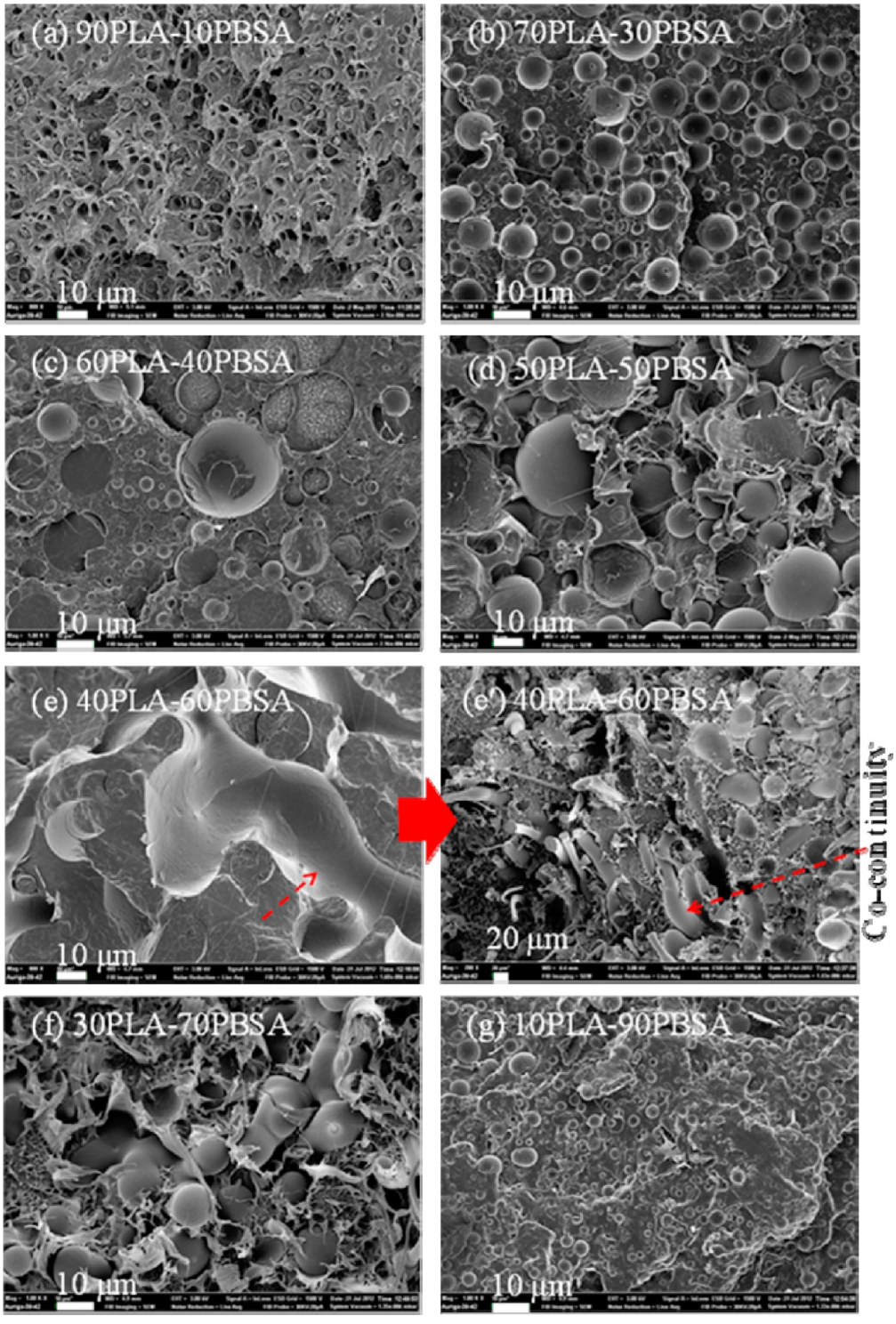

Figure 2. (a–g) SEM micrographs of PLA/PBSA blends at different compositions; (e′) low-magnification SEM image of 60/40 sample at a different location from e, illustrating co-continuous morphology. Samples had been annealed at 80 °C for 15 h and fractured by tensile pull.

sample). Therefore, relatively stable morphologies are favored by lower content of the dispersed phase, primarily because the chance of the droplets colliding with one another is reduced, and so is their coalescence.

Even though PLA and PBSA are immiscible, slight adhesion between the phases is possible at the interface of the two polymers because of the possibility of intermingling of their chains. Therefore, this marginal adhesion may be enhanced if the surface area of the dispersed phase exposed to the major matrix is maximized. However, this can only be possible at certain compositions. Compositions where PLA is the major phase, with PBSA forming discrete domains will be used to illustrate this point below.

The average diameter of the domains for selected samples (90PLA/10PBSA, 70PLA/30PBSA, 60PLA/40PBSA, and 50PLA/50PBSA) for which PBSA was dispersed as a discrete domain was determined by the image processing software, ImageJ (NIH, USA), using the following equation

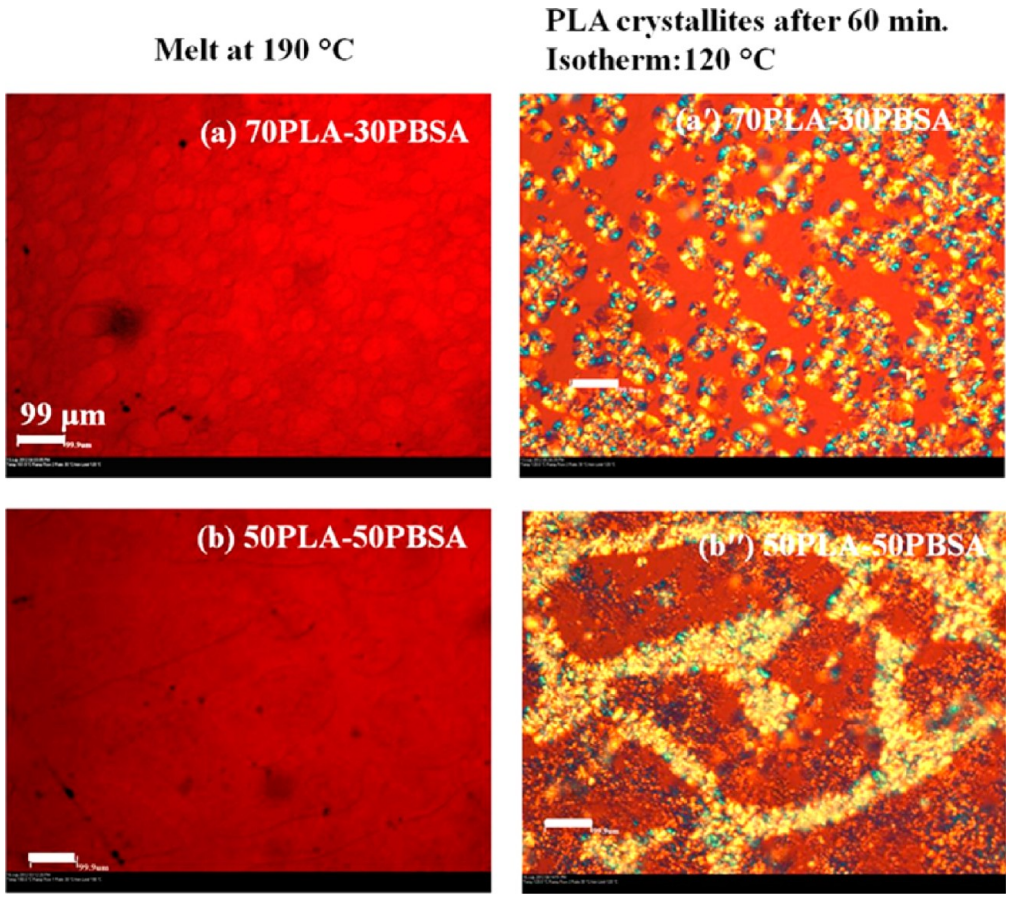

Figure 3. POM micrographs of 70PLA/30PBSA and 50PLA/50PBSA in (a, b) molten state and (a′, b′) after crystallization of PLA component for 60 min at 120 °C.

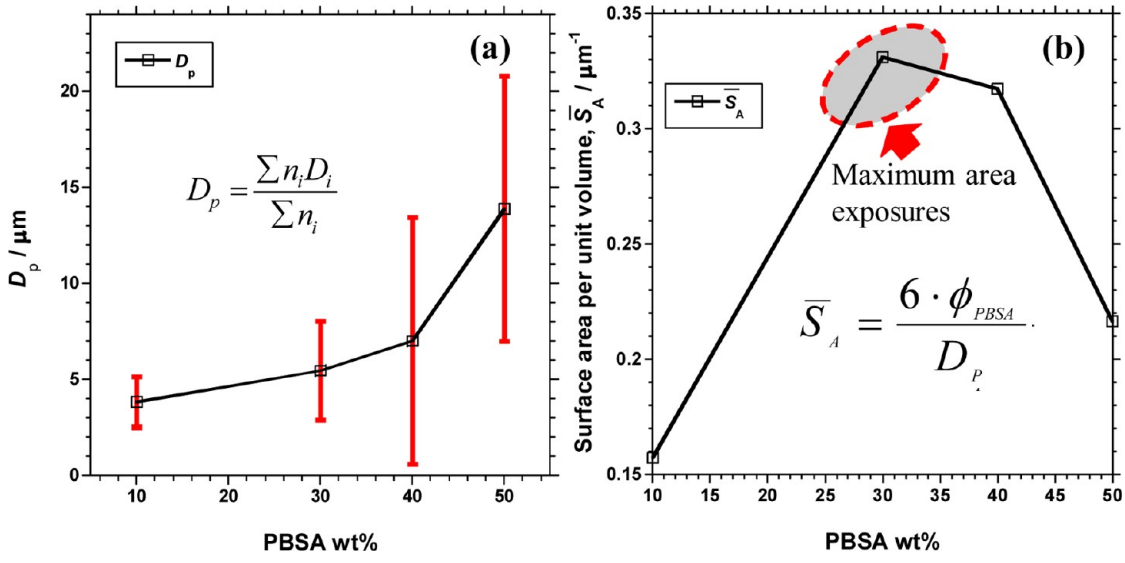

Figure 4. (a) Number average PBSA domain sizes obtained from SEM images in Figure 2. The error bars are for the standard deviations and give an idea of dispersion of the particle size around the reported mean value. (b) Surface area of PBSA domains per unit volume of blend.

$$D_p = \frac{\sum n_i D_i}{\sum n_i} \quad (2)$$

where n_i is the number of the dispersed domains with a diameter of D_i counted from the SEM images in Figure 2.

A plot of the D_p as a function of the weight fraction of PBSA in the blend is as shown in Figure 4a. The domain size increases as PBSA fraction is increased. This is due to the immiscibility of the two polymers, which tend to segregate from each other. As the PBSA fraction was increased, the standard deviation also increased, signifying a broad variation of the sizes around the reported mean value.

Assuming that the dispersed PBSA droplets are spherical, the total surface area exposed by the droplets per unit volumetric space of the blend is given by the following equation

dx.doi.org/10.1021/am301842e | ACS Appl. Mater. Interfaces 2012, 4, 6690−6701

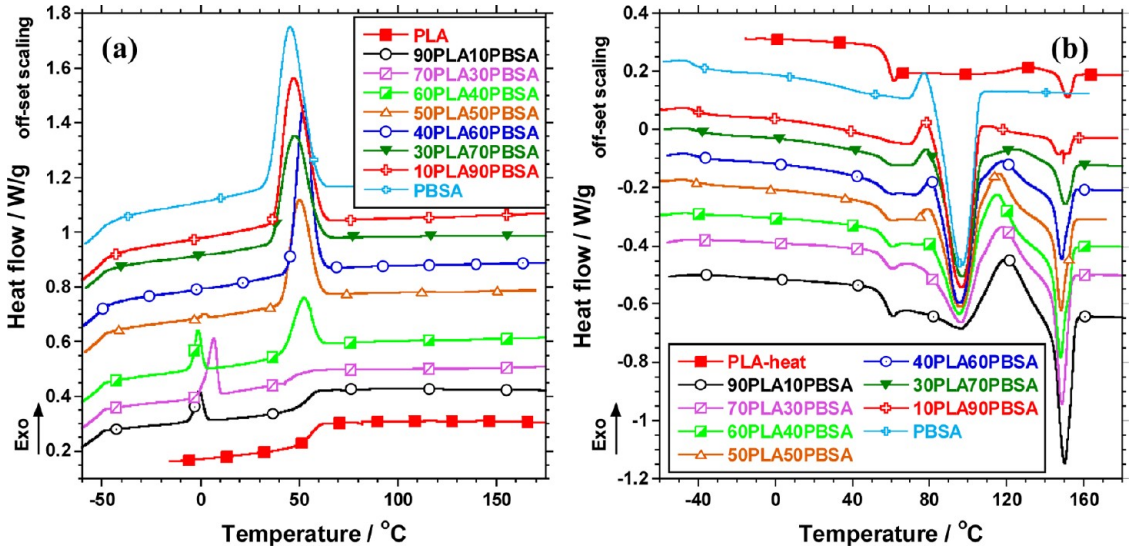

Figure 5. DSC cooling curves and the corresponding heating curves for neat polymers and their blends. The cooling rate and heating rates were both set at 10 °C/min.

$$\bar{S}_A = \frac{6 \cdot \phi_{PBSA}}{D_p} \tag{3}$$

where ϕ_{PBSA} is the volumetric fraction of PBSA in the blend and D_p is the PBSA domain size obtained from eq 2.

From the above expression, two interrelated variables, (i) volume fraction of the dispersed phase and (ii) the size of the droplets of the dispersed phase, have opposite effects on the interfacial area and hence a maximum area is expected as the volume fraction of PBSA is increased. Figure 4b shows a plot of the surface area exposed by the PBSA droplets (interfacial area) per unit volume of the blend as a function of the weight fraction of the PBSA. Expectedly, the specific interfacial area increases with increasing PBSA weight fraction, until a maximum is reached at about 30 wt % PBSA. As the weight fraction of PBSA was increased beyond 30 wt %, the surface area per unit volume was reduced because of the steep increase in the PBSA droplet sizes resulting from coalescence. In conclusion, due to the large exposed surface area per unit volume, it is expected that the best synergies of the properties of the two polymers should be realized in the vicinity of 70/30 model composition, in the case where the dispersed phase is PBSA. Therefore, any work on compatibilization of the PLA/PBSA blends would justifiably be based on blends with weight fraction of PBSA in the region of 30%.

3.2. Thermal Properties. DSC was used to study the thermal properties of the blends. Figure 5a shows the cooling curves of the neat polymers and their blends obtained while cooling the samples at 10 °C/min from 190 °C to −65 °C. On the other hand, Figure 5 (b) shows the corresponding heating curves obtained while heating the samples from −65 °C to 190 °C at 10 °C/min. During cooling, the PLA component hardly crystallizes, since no apparent peaks were noted. On the other hand, PBSA crystallizes either all at once (40/60, 30/70, and 10/90 samples) or in a fractionated fashion with multiple crystallization peaks (70/30, 60/40, and 50/50 samples). Similar fractionated crystallization of PBSA was also reported by Wang and Mano.[42]

On first heating, the samples registered different T_g values, corresponding to PLA and PBSA, although the value of the latter was hardly observable because of the low heating rate used. After melting the PBSA, there was a cold-crystallization of the PLA component, before ultimate melting. For easy visualization, the information from Figure 5b, vis-à-vis the T_g, cold crystallization temperature (T_{cc}), and the melting point (T_m) of PLA were extracted and presented in Figure 6a as a function of the PBSA weight fraction. Clearly, the cold crystallization temperature of PLA decreased with an increase in the PBSA content, in cases where PLA was the major matrix. The T_{cc} of neat PLA of approximately 131 °C was reduced to approximately 115 °C for the 60PLA/40PBSA blend. The peak width was also greatly reduced in the case of blend, signifying enhanced crystallinity. This suggests that PBSA enhanced the ability of PLA to cold crystallize in the PLA-rich blends. Molten PBSA could enhance cold crystallization of PLA, just as it has been shown that molten PBSA can nucleate crystallization of PLA from melt.[46] In cases where PLA was the dispersed phase, the increase in PBSA content had the opposite effect: retardation of crystallization, as shown by the increase in T_{cc}. From the inset in Figure 6a, the T_g of PLA reduces as PBSA was increased. Apart from PBSA enhancing cold crystallization of PLA, the reduced T_g of PLA in the blends implies that the PLA chains are able to soften at lower temperatures than the T_g of neat PLA, allowing cold crystallization to occur at lower temperatures as well. Similarly, the melting temperature was completely dependent on the T_{cc}: that is, the lower the T_{cc}, the lower the T_m and vice versa, because crystals formed at lower temperature were less stable and melted at lower temperatures.

Crystallinity of PLA achieved during cooling (χ_c), cold crystallization (χ_{cc}), and the total crystallinity (χ_m) was calculated by the following expressions and plotted as a function of PBSA weight fraction, as shown in part b of Figure 6

$$\chi_m = \left(\frac{\Delta H_m}{\phi_{PLA}\Delta H_m^o}\right)100;\ \chi_{cc} = \left(\frac{\Delta H_{cc}}{\phi_{PLA}\Delta H_m^o}\right)100 \tag{4}$$

$$\chi_c = \chi_m - \chi_{cc} \tag{5}$$

where ΔH_m is the melting enthalpy, ΔH_{cc} is the enthalpy of cold crystallization, ϕ_{PLA} is the weight fraction of PLA, and ΔH_m^o is the enthalpy of fusion of 100% PLA, taken as 93 J/g.[50]

dx.doi.org/10.1021/am301842e | ACS Appl. Mater. Interfaces 2012, 4, 6690−6701

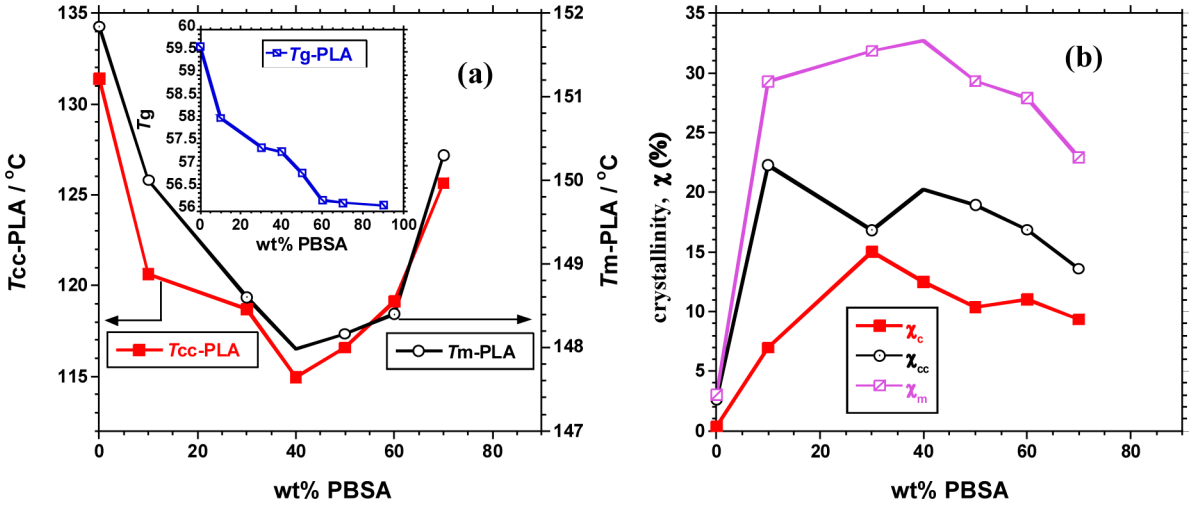

Figure 6. (a) Variation in the cold crystallization temperature, melting point, and T_g of PLA with PBSA content and (b) crystallinity of PLA as a function of PBSA weight fraction, where χ_c and χ_{cc} represent crystallinity achieved during cooling and cold crystallization, respectively, whereas χ_m is the total crystallinity achieved during both processes.

Crystallinity of PLA as a function of the PBSA content is shown in Figure 6b. Crystallinity from melt increased until it peaked when the PBSA weight fraction was 30%. Thereafter, it slowly decreased with further increase in the PBSA content. The total crystallinity rose steeply from 2.9% as the PBSA content was increased until it peaked at around 32% when PBSA content was in the region of approximately 30−40 wt %. Further increase in PBSA concentration resulted in the reduction of the crystallinity of PLA. It is instructive to note that neat PLA used in the study has low crystallinity, which improves with the addition of PBSA. The fact that the crystallinity peaked in the region where PBSA content is approximately 30 wt % is believed to be linked to the interfacial area exposed by the PBSA, which was shown to be a maximum around the same concentration. It is possible that the nucleation of the PLA by the molten PBSA occurs at the interface between the two phases and hence the larger the interfacial area, the better the nucleation and ultimate crystallinity of PLA.

To study the cold-crystallization of the PBSA component, we used high speed DSC equipment with ballistic cooling capability. This is because the PBSA crystallizes very fast and it is not possible to study the cold crystallization with DSC equipment with a controlled cooling rate capability <35 °C/min. The samples were quenched from melt by ballistic cooling to ensure that PLA and PBSA remained in the amorphous state. Thereafter, the samples were heated at 10 °C/min, and the resultant thermograms are shown in Figure 7a. The cold crystallization peak temperature of PBSA, the T_g, and the crystallinity achieved were extracted from the thermograms in Figure 7a and plotted as a function of PBSA content as shown in parts b and c in Figure 7. For the determination of crystallinity of PBSA, the enthalpy of cold crystallization attributed only to the PBSA component was divided by 113.4 J/g, where 113.4 J/g was taken as the enthalpy of fusion for neat PBSA crystal (ideally 100% crystal).[39]

As shown in Figure 7b, the T_g of the PBSA showed a relatively constant value in the PBSA-rich compositions (−40.8 to −39.7 °C). However, the T_g of PBSA was not visible in the PLA-rich blends. Since PLA and PBSA were in the amorphous states, some of the PBSA chains, especially those close to the interface, were intermingled with hard but amorphous PLA component, where the glass transition temperature had not been reached (see the representation of a possible interface intermingling in the insert in Figure 7c). The hard PLA component locked in the PBSA chains intermingled with it at the interface, thus preventing their motion. Because the proportion of the PBSA chains at the interface with PLA was greater for low values of PBSA fraction, the proportion of the chains that are restricted was high and hence the absence of notable T_g of PBSA.

Unlike PLA, PBSA crystallization was not enhanced by the PLA component. This was evident from the values of T_{cc} of PBSA in parts a and b in Figure 7. Interestingly, just like crystallization from melt, cold crystallization of samples with PBSA as the minor phase, two crystallization temperatures were observed (refer to Figure 7a). This phenomenon is attributed to the different heterogeneities present in the droplets, necessitating nucleation at different extents of under-cooling. However, considering only the main T_{cc} of PBSA, it was noted that it was lower in the neat PBSA sample than in any of the blends. In the PBSA-rich blends, the peak of the cold crystallization temperature of PBSA shifted monotonously to the higher temperatures with increasing PLA content. The $T_{cc,\,PBSA}$ was −9.68 °C for neat PBSA and shifted to −0.7 °C for the blend with 40% PLA. This implied that PLA actually impeded crystallization of PBSA. The hard PLA component prevented diffusion of the PBSA chains close to the interface from joining the crystallization front in the PBSA phase. This was expectedly worse for blends with PBSA as the minor matrix, thereby resulting in lower crystallinity as shown in Figure 7c.

Looking at the crystallization behavior of the model blend, 70PLA/30PBSA, it was noted that on cooling from melt, the blend achieved the highest crystallinity of PLA, which is indeed important in enhancing properties such as the modulus, as will be discussed in later sections. In addition to this, the retarded crystallization of PBSA portion that intermingled with PLA at the interface of the two phases helps to enhance the elongation-at-break, making model blend an ideal one.

3.3. Thermogravimetric Analysis (TGA). Thermoxidative degradation analyses were performed on the blends that had been previously annealed at 80 °C for 15 h. Figure 8a shows the plot of relative weight loss as a function of temperature. For a clear visualization of the degradation process, the first derivative TGA (dTGA) curves of the blends were plotted as a function of

dx.doi.org/10.1021/am301842e | ACS Appl. Mater. Interfaces 2012, 4, 6690−6701

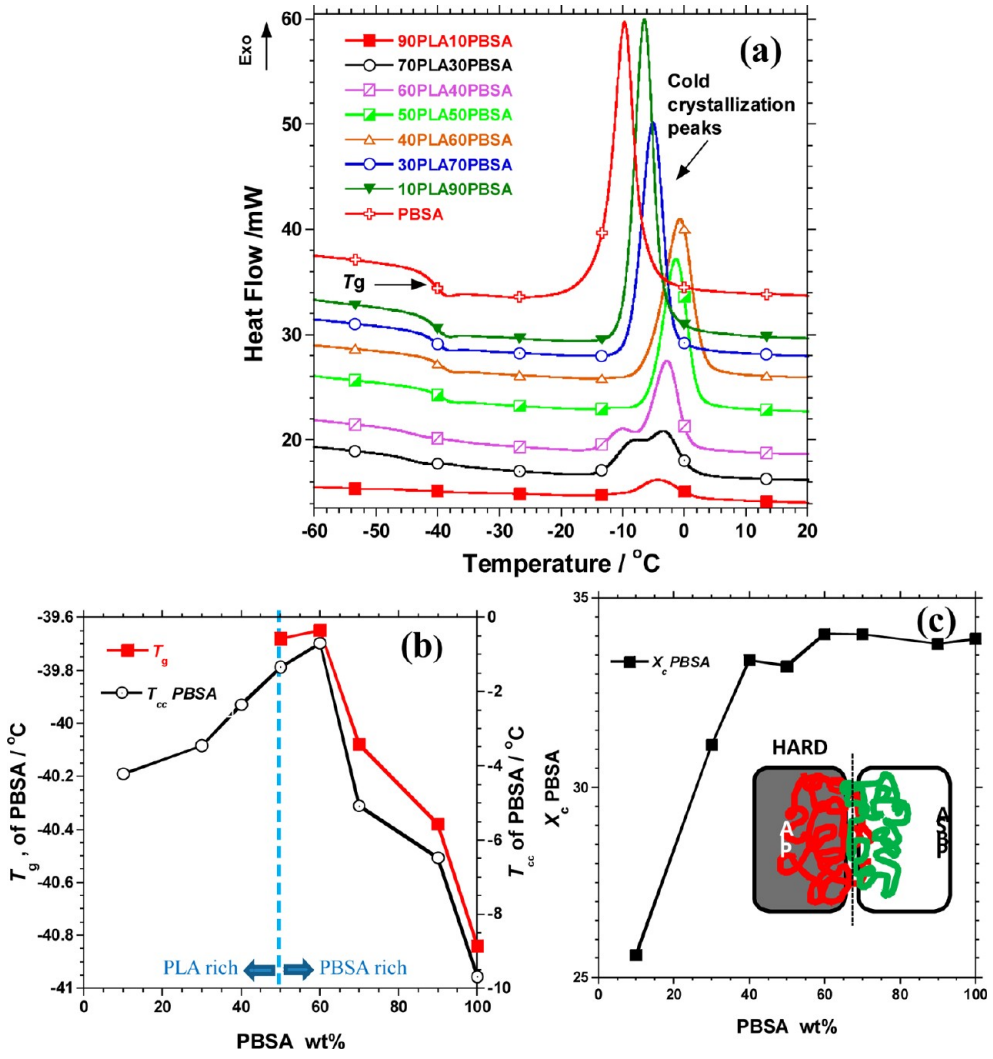

Figure 7. (a) DSC heating curves showing cold crystallization peaks of PBSA component for the various blend compositions (b) T_g and T_{cc} values of PBSA component as a function of PBSA weight fraction, and (c) crystallinity achieved on cold crystallization as a function of PBSA weight fraction.

temperature as shown in Figure 8b. The onset degradation temperature, T_5, taken arbitrarily as the temperature at which 5% degradation occurred; T_{50}, the temperature after 50% degradation, were obtained from three individual tests per sample and the average values plotted as a function of temperature as shown in Figure 8a′. The standard deviation values are shown as error bars. On the other hand, the temperatures at which maximum rate of degradation occurred for the PLA component, T_{max}I and for the PBSA component, T_{max}II were also obtained from the three tests and the average plotted as a function of temperature as shown in part b′ of Figure 8.

PBSA has greater thermal stability than PLA as evident from the higher T_5 and T_{max} values. On blending the two, one would expect to have thermal stabilities in between those of neat polymers. However, this was not the case, and the thermal stability of the blends tended to be lower than those of the neat polymers. In the PLA-dominated blends, the onset of degradation seemed to be highly correlated with the morphologies observed in the SEM image (refer to Figure 2). As the coarseness in the morphology got worse in the PLA-dominated blends with the addition of PBSA, so did the average T_5 implying that fine morphology was necessary for maintaining thermal stability. For the PBSA-dominated blends, it is not clear at the moment why the average T_5 was not, at least, better than that of neat PLA, but could be due to the rather poor morphologies obtained (refer to parts e and f in Figure 2). On the other hand, there was a general increase in the value of T_{50} as PBSA content was increased because PBSA is more thermally stable than PLA. With the degradation of the PLA component starting at lower temperatures, the remaining component was the higher stable PBSA, hence the increase in T_{50} and T_{90} values with an increase in the PBSA content.

We again see the effect of the morphology on the maximum degradation temperatures as shown in Figures 8b, b′. The average T_{max}I was even slightly better than that of the neat PLA when the PBSA content was less than 30 wt %. Beyond 30 wt % of PBSA, the T_{max}I reduced drastically because of the poor morphology. This fact affirms the suitability of 70PLA/30PBSA blend as being the optimal blend. Unlike PLA-rich blends, PBSA-rich blends save for the 10PLA/90PBSA blend, showed two separate maximum degradation peaks associated with PLA and PBSA. The T_{max}I in PBSA-rich blends was lower than the T_{max}I in the PLA-dominated blends. However, the T_{max}II in the PBSA-rich blends increased with the increase in PBSA content. This is consistent with the lower crystallinity of the PLA component in the PBSA-rich blends, when compared to the PLA-rich blends, as well as the enhanced crystallinity for PBSA component for the PBSA-dominated blends. The two-step degradation in the

dx.doi.org/10.1021/am301842e | ACS Appl. Mater. Interfaces 2012, 4, 6690−6701

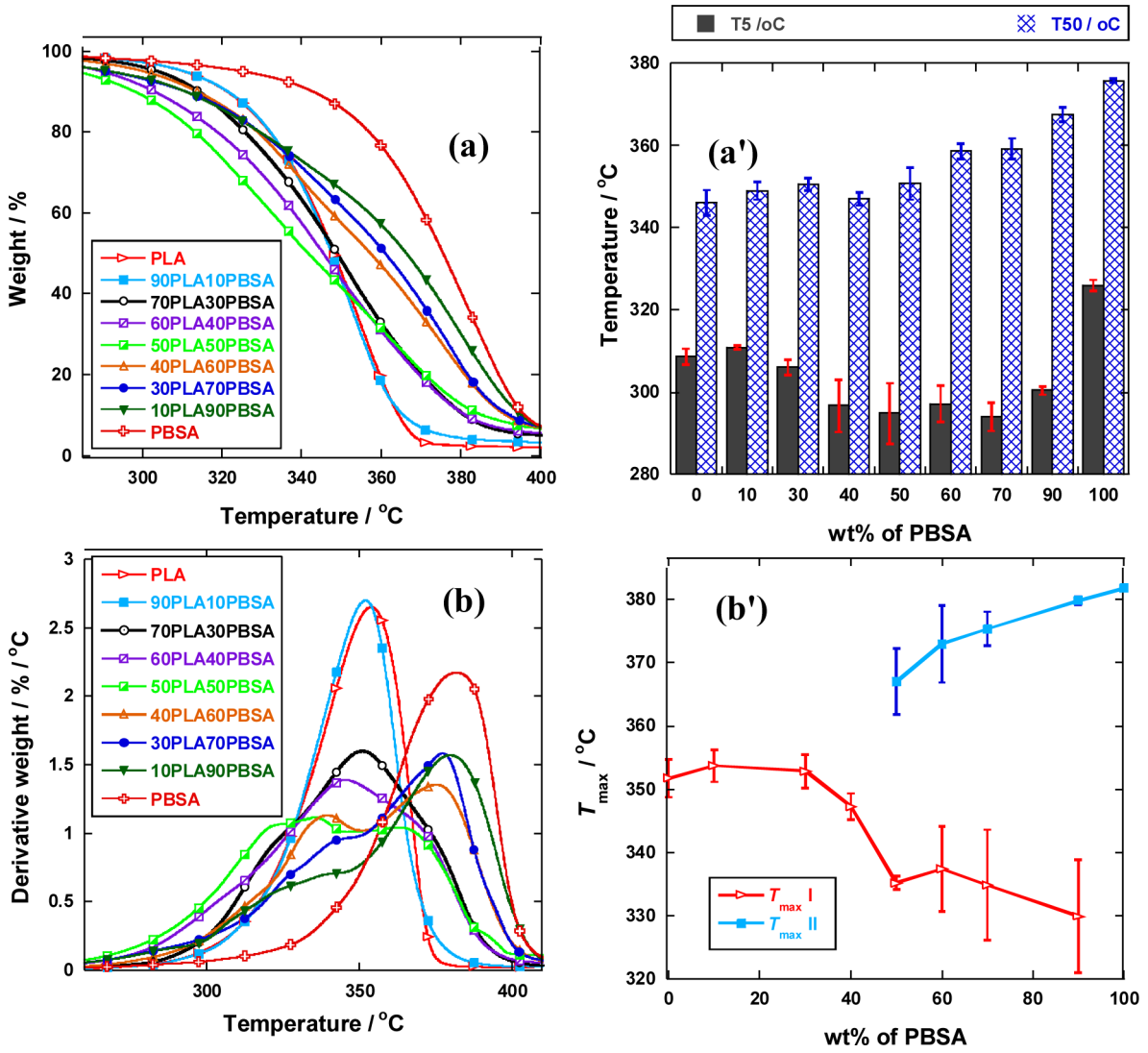

Figure 8. (a) Typical TGA traces of the relative weight loss as a function of temperature; (a′) extracted information from part a: the onset degradation temperatures (T_5), temperature after 50% (T_{50}) and 90% (T_{90}) degradation as a function of the PBSA weight fraction; (b) first derivative TGA (dTGA) curves of the blends and (b′) plots of maximum degradation temperatures associated with PLA (T_{max}I) component and PBSA (T_{max}II) component as a function of PBSA content.

PBSA-rich blends also shows that indeed, phase separation, either through flow-induction or the subsequent annealing of samples, was more severe in PBSA-dominated blends than in the PLA-dominated blends.

In conclusion, the phase morphology has been correlated with thermal stability of the blend and found to especially influence the onset and the maximum degradation temperatures. As mentioned before, blends with less than 30 wt % PBSA showed the least reduction in thermal stability, and a single degradation step, and hence presumably optimal composition, should ideally be in that region: <30 wt % PBSA content.

3.4. Mechanical Properties. The dynamic mechanical analyses (DMA) of the blends were carried out on samples that had been previously annealed at 80 °C for 15 h, and the temperature dependence of the storage modulus (E') is shown in Figure 9a. For better visualization of Figure 9a, the flexural moduli at various temperatures: (i) −65 °C designated region (I), (ii) 20 °C, designated region (II), and (iii) 40 °C, designated region (III) were plotted as a function of PBSA content in Figure 9a′. Region (I) is below the T_g of PLA and PBSA and hence both were in a glassy state. As such, the values of E' for the neat polymers were not very different: 3.4 and 3.77 GPa for PLA and PBSA, respectively. In the glassy state, the molecules of both polymers had limited chain mobility because of the relatively low internal energy, hence the high values of E'. The blends with various compositions also did not show large differences in the values of E', as shown in curve (I) in Figure 9a′. However, further heating beyond the T_g of PBSA resulted in enough internal energy to allow the PBSA chains and chain segments to move freely, lowering the stiffness to a great extent in the process. However, the PLA component was still glassy in regions (II) and (III) and was largely responsible for the stiffness in the blends. From the curve (II) in Figure 9a′, the value of E' almost linearly reduces from 2.7 GPa for the PLA to 0.378 GPa for PBSA. At 40 °C, the trend in the variation of E' with PBSA content was the same, but with slightly lower values. This finding shows that the flexural modulus in the PLA/PBSA blends, near room temperature region, is mostly dependent on the content of the constituent polymers. Therefore, in order not to lose the stiffness especially in region (II) in which materials made of blends of

dx.doi.org/10.1021/am301842e | ACS Appl. Mater. Interfaces 2012, 4, 6690−6701

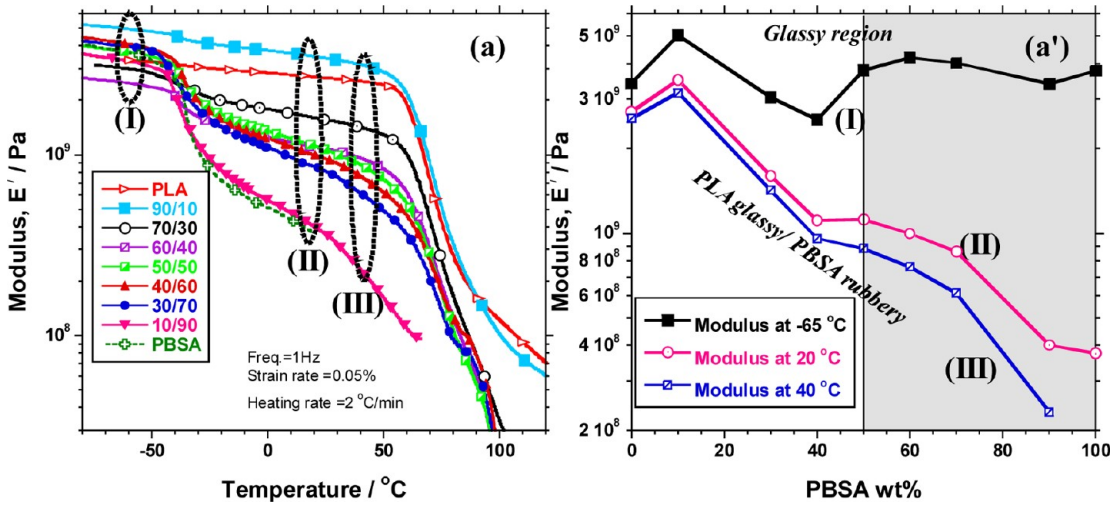

Figure 9. (a)Temperature dependence of the storage modulus (E') for the neat polymers and the polymer blends and (a′) plots of the values of (E') extracted from part a at different temperatures: (I) −65, (II) 20, and (III) 40 °C as a function of PBSA content.

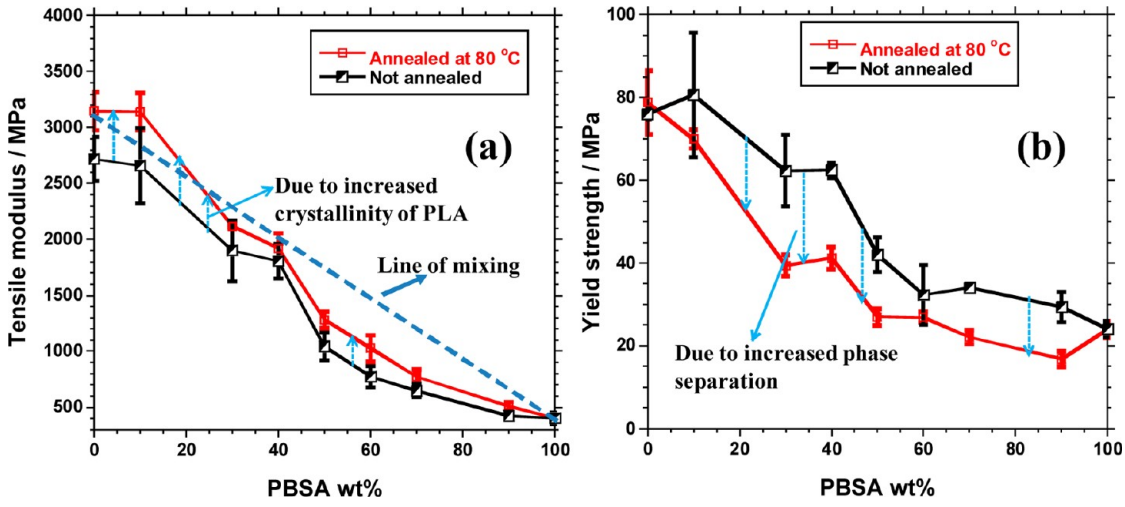

Figure 10. (a) Tensile modulus and (b) strength-at-yield of the blends as a function of the PBSA content for annealed (80 °C for 15h) and unannealed samples. Plotted values are averages of six independent tests with standard deviations as error bars.

PLA/PBSA would most likely be used, the weight fraction of PBSA would need to be as minimal as possible. As a compromise for other properties like elongation-at-break, an adequate amount of PBSA would be needed, as will be seen shortly and the previously identified optimal 70PLA/30PBSA blend would still have adequate stiffness.

Figure 10 shows the tensile modulus and strength-at-yield for the blends as a function of PBSA content. In addition, Figure 11 shows the elongation-at-break for the blends and typical stress-strain curves depicting the type of fracture as a function of PBSA content. The modulus decreased with the addition of PBSA, since at room temperature (at which the tensile tests were carried out), PLA was stiffer than PBSA, as has been shown in the DMA analysis. However, the trend did not follow the "rule of mixtures" line expected of blends with good interfacial adhesion. This further shows the immiscibility of the two polymers. In the PLA-dominated blends, the experimental modulus values straddled the values predicted from the "rule of mixtures" line, with certain compositions such as 90/10 showing a better modulus value than the predicted one. On the other hand, PBSA-dominated blends showed the worst fit to 'rule of mixtures' line. This is attributed to the coarser morphology of the PBSA-dominated blends when compared to the relatively fine morphology of the PLA-dominated blends with corresponding but opposite compositions (refer to SEM images in Figure 2). The hindrance to the transfer of stress from one phase to the other was, therefore, worse in PBSA-dominated blends than PLA-dominated blends.

Obviously, the main factors that would affect the resultant modulus of the blends are (i) the modulus of each component, (ii) the composition of the blend, (iii) the interfacial adhesion between the components and hence the morphology, and (iv) the crystallinity of the components. Crystallinity of the PLA component was enhanced through the annealing of the blends at 80 °C for 15 h. The moduli of the two sets of samples, annealed and un-annealed, were compared as shown in the Figure 10a. Crystallization through annealing increased the packing density of the PLA component, hence stiffening the chains and resulting in higher modulus values than the softer un-annealed blends. The change in the modulus due to crystallization was, therefore, expectedly higher in the PLA-rich blends than it was in PBSA-rich blends.

Similarly, the strength-at-yield of the blends generally reduced with increasing PBSA content, since PLA had higher strength (78.8 MPa) than PBSA (24 MPa) as shown in Figure 10b.

dx.doi.org/10.1021/am301842e | ACS Appl. Mater. Interfaces 2012, 4, 6690−6701

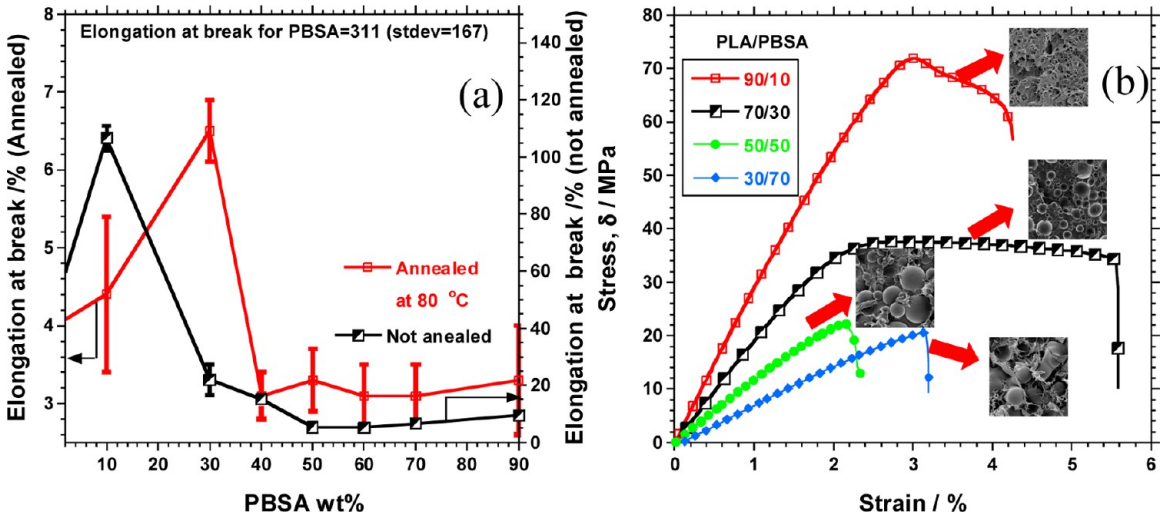

Figure 11. (a) Elongation at break of blends as a function of temperature and annealing process and (b) typical stress-strain curves showing failure type for selected blends. The SEM images shown were obtained from Figure 2.

However, on annealing the samples, the yield strength of the blends reduced, with the PLA-dominated blends posting bigger reduction than PBSA-dominated blends. The reduction in the yield strengths is attributed to the worsening phase separation induced by the crystallization of the PLA component during the annealing process. Due to the phase separation, load transfer between the phases was hindered resulting in early failures at the de-bonded interfaces.

In Figure 11a, the elongation at break was greatly reduced by the annealing process, as was expected. For instance, amorphous PLA had an elongation at break of 48.8 %, and this decreased to about 4% after annealing. This result was expected since crystallization stiffens the polymer chains, leaving little room for them to stretch when pulled. Annealed samples will be used to discuss the effect of PBSA weight fraction on the blends, since they have more stable morphologies than the amorphous samples. As PBSA content was increased, it would have been expected that the elongation-at-break values would increase too, since PBSA has better elongation-at-break (311%) than PLA (4%, for the annealed sample). However, this was not the case, with the only enhancement in elongation-at-break over that of neat PLA being observed in blends with less than 30 wt % PBSA. It was previously discussed that in the PLA-dominated blends, maximum specific interfacial area exposed by the dispersed PBSA phase was found in the blend with 30 wt % PBSA. As such, even though the two polymers are immiscible, the extent of some chains from both polymers intermingling at the interface would be maximal for the 70/30 blend. These intermingled chains at the interface acted as the bridge between the PLA and PBSA phases, thereby transferring the ductility of PBSA to the whole blend. Indeed, the elongation-at-break for the 70/30 blend was the highest at 6.5% when compared to 4% for neat PLA and 3.3% for the 50/50 blend. Typical stress−strain plots for the blends shown in Figure 11b illustrate the relatively ductile fracture for the 70/30 blend when compared to the brittle failure in the case of the blend with 50 and 70 wt % PBSA. At the moment, one of the probable reasons given for the unexpected reduction in the elongation-at-break values in the PBSA-dominated blends is the poor morphologies of such blends, although the exact reason is not known. As discussed earlier, the lower viscosity of PBSA, when compared to that of PLA at the processing temperature of 185 °C, made it difficult for the PBSA to deform the PLA phase, resulting in poorer morphologies, which invariably resulted in poor ductility. For instance, the SEM image of 30PLA/70PBSA blend showed bigger and smooth-surfaced dispersed phase when compared to 70PLA/30PBSA blend. The smooth surface depicted easy debonding of the phases during tensile pull.

In conclusion, 70PLA/30PBSA blend showed a slight increase in the elongation-at-break, with a ductile failure type occurring, when compared to the brittle fractures in other blends. Even though such improvement was small, it re-enforces the earlier hypothesis about the specific interfacial area being important in maximizing the little interfacial adhesion between PLA and PBSA. Further work on compatibilization of the blend with PLA/PBSA ratio around 70/30 should result in better elongation-at-break.

4. CONCLUSIONS

Binary biodegradable blends of PLA and PBSA prepared through the melt-blending process resulted in phase morphologies based on their respective composition. To a large extent, the resultant morphology, and hence the specific interfacial area, dictated the mechanical and thermal properties of the blend. The annealing process, which worsened the phase separation, not only lowered the yield strength but also resulted in reduced elongation-at-break of the blends. However, even with annealing, blends with composition in the region of 70PLA/30PBSA showed a slight increase in elongation at break over that of annealed PLA. The increase in elongation-at-break for the 70PLA/30PBSA blend was attributed to the large specific interfacial area exposed by the dispersed PBSA phase, which allowed for maximum intermingling of the chains of the otherwise immiscible polymers. Because of the slight increase in elongation-at-break and only slight reduction in the modulus and thermal stability, 30 wt % PBSA in a PLA/PBSA blend is considered to be the optimal composition. The problem of brittleness of PLA is mitigated at this composition, while at the same time; the loss of the inherent strength of PLA is not severe. Further work on compatibilization of the 70PLA/30PBSA blend is envisaged to produce an even better blend with properties of the two polymers synergized.

AUTHOR INFORMATION

Corresponding Author

*Fax: +2712841 2229. E-mail: RSuprakas@csir.co.za.

Notes

The authors declare no competing financial interest.

■ ACKNOWLEDGMENTS

S.S.R. and V.O. thank the Technology Innovation Agency, Republic of South Africa for financial support.

■ REFERENCES

(1) Sinha Ray, S.; Bousmina, M. *Prog. Mater. Sci.* **2005**, *50*, 962.
(2) Auras, R.; Harte, B.; Selke, S. *Macromol. Biosci.* **2004**, *4*, 835.
(3) Drumright, R. E.; Gruber, P. R.; Henton, D. E. *Adv. Mater.* **2000**, *12*, 1841.
(4) Ikada, Y.; Tsuji, H. *Macromol. Rapid Comm* **2000**, *21*, 117.
(5) Ikada, Y. *Adv. Eng. Mater.* **1999**, *1*, 67.
(6) Vert, M. *Macromol. Symp.* **2000**, *153*, 333.
(7) Ouchi, T.; Ohya, Y. *J Polym. Sci., Part A: Polym. Chem.* **2004**, *42*, 453.
(8) Amass, W.; Amass, A.; Tighe, B. *Polym. Int.* **1998**, *47*, 89.
(9) Hoshino, A.; Isono, Y. *Biodegradation* **2002**, *13*, 141.
(10) Perepelkin, K. E. *Fibre Chem* **2002**, *34*, 85.
(11) Dorgan, J. R.; Lehermeier, H. J.; Palade, L.-I.; Cicero, J. *Macromol. Symp.* **2001**, *175*, 55.
(12) Żenkiewicz, M.; Rytlewski, P.; Malinowski, R. *J. Achieve. Mater. Manuf. Eng.* **2010**, *43*, 192.
(13) Van de Velde, K.; Kiekens, P. *Polym. Test.* **2002**, *21*, 433.
(14) Wu, D.; Zhang, Y.; Zhang, M.; Zhou, W. *Eur. Polym. J.* **2008**, *44*, 2171.
(15) Wang, L.; Ma, W.; Gross, R. A.; McCarthy, S. P. *Polym. Degrad. Stab.* **1998**, *59*, 161.
(16) Wu, D.; Lin, D.; Zhang, J.; Zhou, W.; Zhang, M.; Zhang, Y.; Wang, D.; Lin, B. *Macromol. Chem. Phys.* **2011**, *212*, 613.
(17) Broz, M. E.; VanderHart, D. L.; Washburn, N. R. *Biomaterials* **2003**, *24*, 4181.
(18) Chen, C.-C.; Chueh, J.-Y.; Tseng, H.; Huang, H.-M.; Lee, S.-Y. *Biomaterials* **2003**, *24*, 1167.
(19) Kodama, Y.; Machado, L. D. B.; Giovedi, C.; Nakayama, K. *Nucl. Instrum. Meth. Phys. Res., Sect. B* **2007**, *265*, 294.
(20) López-Rodríguez, N.; López-Arraiza, A.; Meaurio, E.; Sarasua, J. R. *Polym. Eng. Sci.* **2006**, *46*, 1299.
(21) Todo, M.; Park, S. D.; Takayama, T.; Arakawa, K. *Eng Fract. Mech.* **2007**, *74*, 1872.
(22) Tsuji, H.; Ikada, Y. *J. Appl. Polym. Sci.* **1996**, *60*, 2367.
(23) Meredith, J. C.; J. Amis, E. *Macromol. Chem. Phys.* **2000**, *201*, 733.
(24) Yeh, J.-T.; Yang, M.-C.; Wu, C.-J.; Wu, C.-S. *J. Appl. Polym. Sci.* **2010**, *112*, 660.
(25) Jiang, L.; Wolcott, M. P.; Zhang, J. *Biomacromolecules* **2005**, *7*, 199.
(26) Gu, S.-Y.; Zhang, K.; Ren, J.; Zhan, H. *Carbohydr. Polym.* **2008**, *74*, 79.
(27) Zhang, N.; Wang, Q.; Ren, J.; Wang, L. *J. Mater. Sci.* **2009**, *44*, 250.
(28) Kanzawa, T.; Tokumitsu, K. *J. Appl. Polym. Sci.* **2011**, *121*, 2908.
(29) Han, L.; Han, C.; Zhang, H.; Chen, S.; Dong, L. *Polym. Compos.* **2012**, *33*, 850.
(30) Zhao, Q.; Wang, S.; Kong, M.; Geng, W.; Li, R. K. Y.; Song, C.; Kong, D. *J. Biomed. Mater. Res., B: Appl. Biomater.* **2011**, *100B*, 23.
(31) Zhang, K.; Mohanty, A. K.; Misra, M. *ACS Appl. Mater. Interfaces* **2012**, *4*, 3091.
(32) Liu, X.; Dever, M.; Fair, N.; Benson, R. *J. Polym. Environ.* **1997**, *5*, 225.
(33) Park, J. W.; Im, S. S. *J. Appl. Polym. Sci.* **2002**, *86*, 647.
(34) Bhatia, A.; Gupta, R. K.; Bhattacharya, S. N.; Choi, H. J. *J. Appl. Polym. Sci.* **2009**, *114*, 2837.
(35) Pucci, A.; Signori, F.; Bizzarri, R.; Bronco, S.; Ruggeri, G.; Ciardelli, F. *J. Mater. Chem.* **2010**, *20*, 5843.
(36) Shibata, M.; Inoue, Y.; Miyoshi, M. *Polymer* **2006**, *47*, 3557.
(37) Yokohara, T.; Yamaguchi, M. *Eur. Polym. J.* **2008**, *44*, 677.
(38) Montaudo, G.; Rizzarelli, P. *Polym. Degrad. Stab.* **2000**, *70*, 305.
(39) Ahn, B. D.; Kim, S. H.; Kim, Y. H.; Yang, J. S. *J. Appl. Polym. Sci.* **2001**, *82*, 2808.
(40) Nikolic, M. S.; Djonlagic, J. *Polym. Degrad. Stab.* **2001**, *74*, 263.
(41) Lee, S.; Lee, J. W. *Korea-Aust. Rheol. J.* **2005**, *17*, 71.
(42) Wang, Y.; Mano, J. F. *J. Appl. Polym. Sci.* **2007**, *105*, 3204.
(43) Wang, R.; Wang, S.; Zhang, Y. *J. Appl. Polym. Sci.* **2009**, *113*, 3630.
(44) Wang, R.; Wang, S.; Zhang, Y. *J. Appl. Polym. Sci.* **2009**, *113*, 3095.
(45) Eslami, H.; Kamal, M. R. *J. Appl. Polym. Sci.* **2012**, *127*, 2290.
(46) Ojijo, V.; Cele, H.; Sinha Ray, S. *Macromol. Mater. Eng.* **2011**, *296*, 865.
(47) Ojijo, V.; Malwela, T.; Sinha Ray, S.; Sadiku, R. *Polymer* **2012**, *53*, 505.
(48) Ojijo, V.; Sinha Ray, S.; Sadiku, R. *ACS Appl. Mater. Interfaces* **2012**, *4*, 395.
(49) Briscoe, B. J.; Lawrence, C. J.; Mietus, W. G. P. *Adv. Colloid Interface Sci.* **1999**, *81*, 1.
(50) Tsuji, H.; Ikada, Y. *Polymer* **1995**, *36*, 2709.